IEEE Access
Multidisciplinary ⋮ Rapid Review ⋮ Open Access Journal

Received March 22, 2019, accepted April 12, 2019, date of publication April 22, 2019, date of current version May 1, 2019.

Digital Object Identifier 10.1109/ACCESS.2019.2912317

A Heuristic Approach for Tracking Error and Energy Consumption Minimization in Solar Tracking Systems

DIEGO A. FLORES-HERNÁNDEZ[1], SERGIO I. PALOMINO-RESENDIZ[1,2], ALBERTO LUVIANO-JUÁREZ[1], NORMA LOZADA-CASTILLO[1], AND OCTAVIO GUTIÉRREZ-FRÍAS[1]

[1]Instituto Politécnico Nacional, Unidad Profesional Interdisciplinaria en Ingeniería y Tecnologías Avanzadas, Mexico City 07340, Mexico
[2]Instituto Politécnico Nacional, Escuela Superior de Ingeniería Mecánica y Eléctrica UP Zacatenco, Mexico City 07738, Mexico

Corresponding author: Diego A. Flores-Hernández (dfloreshe@ipn.mx)

This work was supported in part by the Secretaría de Investigación y Posgrado - IPN and Conacyt under Grant SIP-20181665, Grant SIP-20181635, Grant SIP-IPN 20196079, Grant SIP-IPN 20196058, Grant SIP-IPN 20196059, Grant SIP-20181146, Grant SIP-20195901, and Conacyt PN 2016-2551.

ABSTRACT This paper proposes a methodology for optimizing a class of robotic solar tracking systems with two degrees of freedom using a heuristic approach. The proposal allows a balance to be found between the energy consumption and tracking accuracy in the tracking system. The main purpose is the behavior modification of the system through the combination of two manipulation strategies, one associated with the energy savings and the other with the tracking error. The heuristic approach was implemented in a solar tracking system with the end effector connected to a solar measurement device. Four energy-saving strategies and three tracking strategies were developed, simulated, and implemented in the system. The simulation results show that the resulting strategy combination (tracking error and energy saving approach) led to 31.55% energy savings compared to the reference values, with a tracking error of 0.06°. Moreover, the experimental assessment of the same combination led to 26.98% energy is being saved, with an azimuthal tracking error of 0.062° and elevation tracking error of 0.071°. The preceding values support the aim of the presented proposal to significantly reduce energy consumption while concurrently achieving a competitive tracking error.

INDEX TERMS Energy consumption, heuristic optimization, solar tracking system, tracking error.

I. INTRODUCTION

The electrical energy supply at the global level has become an ongoing concern due to the scarcity and high cost of nonrenewable energy sources. The studies presented in [1] foretell an increase in energy demand by 58% between 2004 and 2030. Renewable energy generation is projected to increase 139%, reaching 1, 650 billion kilowatt-hours (BkWh) by 2050 [2]; solar energy is considered as the most promising technology to be developed in the short term due to the considerable increase in its conversion efficiency and its relative cost reduction in the recent years. However, the overall transformation efficiency is still low, on the order of 10^{-2} [3]. Therefore, it is necessary to develop new systems and methods that improve the efficiency of solar energy generation technologies. Some studies have focused on improving the efficiency of the process of converting solar energy into electrical energy using the solar concentration technologies, new materials for solar cells, multijunction technologies, and hybrid systems, among others [4]–[6]. Other studies seek to increase the performance of existing conversion methods, developing solar tracking systems (STSs), novel tracking algorithms, and advanced sensors, among others [7], [8]. Both approaches are related, as the new energy generation technologies demand optimal systems that ensure and increase their energy generation performance. This performance is related mainly to the solar tracking action through energy consumption and tracking error minimization, involving a delicate trade-off between them, as the reduction in tracking error is usually accompanied by an increase in

The associate editor coordinating the review of this manuscript and approving it for publication was Bijoy Chand Chand Chatterjee.

energy consumption. However, these requirements have been addressed independently, as some proposals increase the energy generation performance with implementation of control tracking strategies and more accurate tracking algorithms. The preceding objectives increase the computational performance of the system [9], [11]. Nevertheless, large-scale data processing and more computational effort are required to execute the algorithm, which directly affects the system energy consumption. Additionally, the cited studies do not include an energy consumption analysis [12]–[14]. Other approaches demonstrate an improvement in energy consumption but do not determine the tracking error [15]–[17]. To include both aspects, in this article a heuristic approach is proposed that solves and optimizes, in an integral manner, the trade-off between a high tracking accuracy and a low energy consumption in STSs, finding a harmonic balance through the combination of the best tracking and energy saving schemes. The proposed approach was verified through both numerical and experimental assessments in a tracking system.

The paper is organized as follows. Section II briefly describes the fundamentals of STSs, tracking error, and energy consumption. In Section III, the problem statement of the proposed approach is presented. Section IV describes the proposed heuristic approach. The proposed approach is implemented in a case study presented in Section V. Finally, Section VI concludes the paper.

II. FUNDAMENTALS

A. SOLAR TRACKING SYSTEMS

STSs seek the optimal position of a solar tracking device to take maximum advantage of solar radiation through the alignment of the solar collector orthogonally to sunlight during the daylight period. Common applications that require tracking systems include photovoltaic (PV) systems, concentrated photovoltaics (CPVs), microconcentrator photovoltaics, solar pointing devices, and measuring systems [18]. On the one hand, based on the types of movements performed to follow the sun, there are two types of tracking configurations [14], [19], [20]. First, the one-axis configuration makes the movement from east to west along the solar trajectory, and it has three possible orientations: horizontal, vertical and tilted. This configuration does not have a high accuracy as a result of changes in the solar trajectory with seasons of the year. The second is the two-axis configuration. It allows the alignment with the solar trajectory throughout the year and tracks east to west with one axis and north to south with the second. The two-axis configuration has three main axis arrangements: azimuth-elevation, equatorial with elevation, and portable.

On the other hand, there exists a complementary classification based on the method for sun tracking, which is composed of three configurations: open-loop, closed-loop and mixed. The open-loop configuration uses an algorithm that does not require a feedback of the position of the sun, which reduces the complexity and cost of the system since no additional components or processing are required. Because this configuration does not receive information from the environment, it cannot correct possible errors along its trajectory. Therefore, it cannot compensate for the disturbances, such as wind loads or physical tracker errors. This approach is based on the calculation and prediction of the solar vector, and the system follows the trajectory regardless of the cloud cover. Table 1 shows the main used tracking algorithms, including the year each algorithm was developed, and the tracking error. The closed-loop configuration uses additional devices that allow detecting the sun position in the sky. This approach increases the complexity of the tracker control and the energy consumption of the actuators and electronic components. The accuracy depends on the sensitivity and robustness of the sensors and the tracking control strategy. In adverse conditions in the presence of snow, rain and dust, unsatisfactory results are obtained. Under these conditions, the STS probably loses the position of the sun. The common sensors used include LDR, photoelectric sensors, photovoltaic cells and cameras [12], [21]–[23]. In addition, the common tracking control strategies used are proportional-integral (PI) controller, proportional-integral-derivative (PID) controller, fuzzy logic, neural networks, maximum power operation point (MPOP), artificial vision, maximum power point tracking (MPPT), and sliding modes, among others [24]–[29]. Due to active tracking, this configuration reduces some physical errors such as assembly and manufacturing errors, installation and alignment errors, inaccurate calibration, and deflection errors. Finally, the mixed configuration is a combination of the open-loop and closed-loop configurations. This approach allows the advantages of both configurations to be obtained. Mixed configurations require a management strategy for switching configurations and making decisions. According to experimental results presented in [30], the trackers in open-loop configurations perform better in terms of the control scheme simplicity, the possibility of implementing optimization strategies of

TABLE 1. Algorithms for solar tracking.

Algorithm	Year	Error [deg]	Ref.
Cooper	1969	-	[31]
Spencer	1971	0.25	[32]
Swift	1976	-	[33]
Pitman and Vant-Hull	1978	0.02	[34]
Walraven	1978	0.013	[35]
Archer	1980	-	[36]
Holland and Mayer	1988	-	[37]
Michalsky	1988	0.011	[38]
Blanco-Muriel (PSA)	2001	0.008	[39]
Reda and Andreas (SPA)	2003	0.0003	[40]
Grena (ENEA)	2007	0.0027	[41]
Grena-II (ENEA)	2012	0.190 0.034 0.094 0.0027	[42]

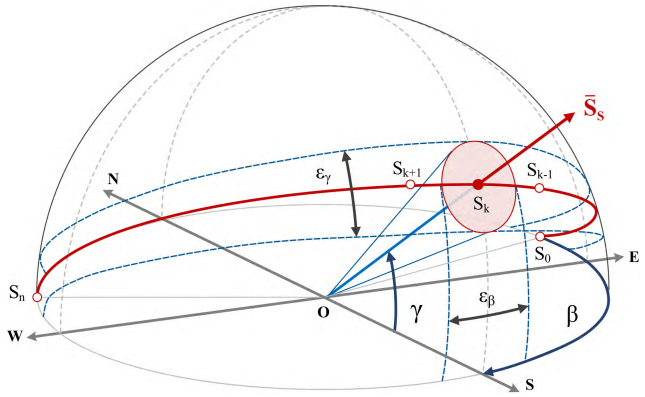

FIGURE 1. Scheme of tracking the sun trajectory.

the tracking algorithm and a significant reduction in energy consumption.

B. TRACKING ERROR

Fig. 1 illustrates the solar path from an observer **O**, where $\bar{S}_S$ is the solar vector that represents the desired position of the collector alignment with respect to the sun position, β is the azimuthal angle, and γ is the elevation angle. The calculation of these angles depends on the selected tracking algorithm (see Table 1. The trajectory can be defined by a series of points from S_0 at sunrise to S_n at sunset. For a two-axis tracker, each point is defined by the duple of azimuthal and elevation angles and can be expressed as $S_k(\beta_k, \gamma_k)$, where $k = 0, \ldots, n$, and n is the last point of the trajectory. Solar tracking accuracy should be considered a function of the solar receiver and collector sensitivity, and it determines the amount of the harvested solar energy. The admissible range of tracking error allowed depends on the use of solar radiation and is associated directly with the acceptance angle (α_s) of the solar collector, which can be defined as the angle within which a source of light can be moved while still converging at the absorber. To reduce the tracking error, specialists design collectors with a wide acceptance angle, which may reduce their efficiency [43]. This angle is associated with the solar tracking operation and can be expressed as the composition of two angles, the azimuthal (α_β) and elevation (α_γ) acceptance angles. Then, the minimum number of points by angle in the trajectory can be defined by (1):

$$n_\beta = \frac{\beta_{tot}}{\alpha_\beta}, \quad n_\gamma = \frac{\gamma_{tot}}{\alpha_\gamma} \tag{1}$$

where β_{tot} and γ_{tot} are the total displacements of azimuthal and elevation angles, respectively. Therefore, the tracking error can be defined by the difference of the desired position (tracking algorithm values), and the real position (tracking system values), and it is expressed in (2) as:

$$\varepsilon_\beta = \beta_d - \beta_r, \quad \varepsilon_\gamma = \gamma_d - \gamma_r \tag{2}$$

where ε_β and ε_γ are the azimuthal and elevation errors, respectively. Variables β_d and γ_d are the desired angles, and β_r and γ_r are the actual measured angles (see Fig. 1). Hence, the conditions $|\varepsilon_\beta| \leq |\alpha_\beta|$ and $|\varepsilon_\gamma| \leq |\alpha_\gamma|$ must be fulfilled. Considering that $n_\beta = n_\gamma$, the k-point mixed error, denoted by ε_{t_k} in (3), is defined as

$$\varepsilon_{t_k}^2 = \varepsilon_{\beta_k}^2 + \varepsilon_{\gamma_k}^2 \tag{3}$$

Therefore, the total tracking error ε_{tot} is given by (4) as an average of the mixed errors calculated by (3):

$$\varepsilon_{tot} = \frac{1}{n}\sum_{k=1}^{n} \varepsilon_{t_k} \tag{4}$$

C. ENERGY CONSUMPTION

According to [10], the total energy consumption in the sun tracking system $EC_{tot}(t)$ is calculated in general form by (5), and expressed as

$$EC_{tot}(t) = \int_0^t u(\tau)i(\tau)d\tau = \int_0^t |P(\tau)|d\tau \tag{5}$$

where $u(\tau)$ is the voltage, $i(\tau)$ is the current, and $P(\tau)$ is the electrical power of the hardware devices. The energy expenditures can be divided in the following aspects: First, the energy consumed when the system is in movement from point S_{k-1} to point S_k is called operational energy consumption $EC_{op}(t)$. Second, the energy consumed when the system is standing by in position S_k until the sun vector $\bar{S}_S$ approaches the boundaries of the tracking error band is called idle energy consumption $EC_{id}(t)$. After that, the system must be activated again for moving to the next position S_{k+1} (see Fig. 1).Hence, the expression (5) can be calculated by (6):

$$EC_{tot}(t) = EC_{op}(t) + EC_{id}(t) = \int_{\Delta t_{op}} |P_{op}(\tau)|d\tau + \int_{\Delta t_{id}} |P_{id}(\tau)|d\tau \tag{6}$$

where the operational period Δt_{op} can be defined as the time required for the movement from S_{k-1} to S_k, and the idle period Δt_{id} as the time during which the tracking system is waiting to carry out the movement to the next position. $P_{op}(\tau)$ and $P_{id}(\tau)$ represent the electrical power required by the hardware devices during the operational and idle periods, respectively.

III. PROBLEM STATEMENT

In view of the existing compromise between the tracking error and the energy consumption, the problem can be defined as a multiobjective problem [45] composed of two objective functions, one for energy consumption minimization (f_1) and the other corresponding to tracking error minimization (f_2). The aim is to find the best combination of two types of approaches, the energy saving (*ESS*) and the tracking error (*TS*) strategies, that minimizes expressions (4) and (6). The combination is defined by $C(ESS_i, TS_j) = C_{i,j}$. The problem can be solved by the utility function method [46], also known

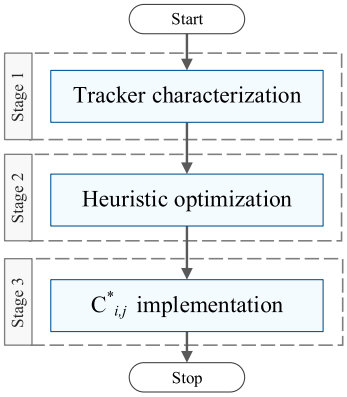

FIGURE 2. General procedure of the heuristic approach to solar tracking systems optimization.

as the weighting function method. Thus, the problem can be stated as finding the optimal combination $C^*_{i,j}$ such that

$$\text{Minimize } U(C_{i,j}) = w_1 f_1(C_{i,j}) + w_2 f_2(C_{i,j}) \tag{7}$$

subject to

$$g_l(C_{i,j}) \leq 0; \quad l = 1, \ldots, r$$

being w_1 and w_2 scalar weighting factors associated with the f_1 and f_2 functions, respectively. Last term is related to the relative importance of each function and it will vary with the tracking application. Thus, a weight should be assigned to each function. And, $g_l(C_{i,j})$ are the inequality and equality constraints. Among the possible constraints defining g_l, the following can be identified:

- Minimum quantity of energy required for activating the functions needed to perform the tracking action,
- Ranges of weather conditions, such as wind speed,
- Hardware device capabilities, such as the number of ports or data processing speed.

The combination $C_{i,j}$ must satisfy the constraints to be considered a feasible combination. To solve the problem, a heuristic approach is proposed [47]. The energy saving efficiency for each combination can be expressed (8):

$$\eta\,(C_{i,j}) = 1 - \frac{EC_{tot}(C_{i,j})}{EC_{tot}(R)} \tag{8}$$

where $EC_{tot}(C_{i,j})$ is the total tracker EC for combination $C_{i,j}$, and $EC_{tot}(R)$ is the total EC of the reference combination R.

IV. THE PROPOSED APPROACH

The proposed heuristic approach seeks to solve the minimization problem stated in (7) by finding combinatorial and approximate solutions based on concepts of the optimization theory. This approach is divided into three stages (see Fig. 2), and each stage is described below.

Stage 1. Tracker characterization: this stage has the main purpose of characterizing the tracking system that will be improved. It is divided into three procedures: First, system identification involves determining the tracking application, the maximum acceptance angle, the tracker configuration, and the device specifications, including the computation of the optimal speed of the axis actuators. Second, tracker modeling deals mainly with the generation of the kinematic and dynamic models. The last procedure is the computation of reference values, $EC_{tot}(t)$ and ε_{tot}. The measurement of energy consumption must be performed for at least the tracking axes, the hardware devices, and the main energy input. Additionally, the measurement of the tracking error must be performed with specialized devices that allow obtaining the values of the azimuthal and elevation angles with an accuracy that should be at least the value of the acceptance angle of the tracking application. These measurements must be made for periods of complete cycles of tracking operation. The obtained tracking error represents the system errors, such as the alignment, assembly, manufacturing, and installation errors.

Stage 2. Heuristic optimization: the proposed approach seeks to find the best combination of energy saving and tracking strategies. According to [44], tracking error strategies are needed to reduce and try to eliminate the tracker errors, such as assembly and fabrication errors, installation and ground leveling errors, inaccurate calibration, and deflections by the loads of the application. Algorithm 1 shows the optimization process. It begins with the generation of the ith energy saving (ESS_i) and the jth tracking (TS_j) strategies, where $i = 1, \ldots, p$ and $j = 1, \ldots, q$, and p, q are positive integers. According to the previous stage and based on the defined constraints, the proposed strategies are evaluated to determine if they can be implemented in the solar tracking system. The strategies must be mutually independent. A *TS* will be feasible as long as the simulation tracking error is equal to or less than the maximum admissible tracking error, complying with the constrains presented in Section II-B. An *ESS* will be feasible if it can be implemented in the existing hardware. In this case, the strategy can be considered for the combinations; otherwise, the strategy is discarded. The proposed strategies may be infeasible, mainly because of requiring physical modifications such as changes of actuators, sensors, or mechanisms, even though they still have the possibility of considerably increasing the performance of the STS; in this case, the modification must be evaluated to determine the possible advantages and the viability of the necessary changes during the tracking system life. Subsequently, the maximum number of feasible combinations K_{max} is determined, and this value will be the algorithm breaking condition. The initial value is $K = 1$. The weights w_1 and w_2 that will transform the multiobjective problem into a single-objective problem are determined. In [46], the definition of the utility function method is presented, and in [48], the interpretation of the weights is developed. The assignment values will depend on the solar tracking system application. If neither the energy consumption nor the tracking error is of greater importance, the assigned values would be 0.5 for both. Otherwise, these properties can be determined by applying a multicriteria selection tool, such as the analytical hierarchy process (AHP), simple additive weighting (SAW), technique

for preference by similarity to the ideal solution (TOPSIS), evolutionary algorithms, fuzzy logic theory, and artificial networks [46], [48]–[50]. In the next part of the algorithm, an iterative evaluation and validation are carried out. The combinations of the strategies are obtained and evaluated in the utility function $U(\mathrm{C}_{i,j})$, see expression (7). The values obtained from the utility function of the new combination ($\mathrm{C}_{\mathrm{new}_{i,j}}$) are directly compared with those for the initial combination ($\mathrm{C}_{\mathrm{ini}_{i,j}}$). If the initial combination is better, the new combination is discarded. Otherwise, the initial combination is discarded, the new combination becomes the initial combination, and a new combination is generated. This process is iterated until the maximum number of combinations is reached, at which point the algorithm is completed, obtaining the best combination of strategies $\mathrm{C}^*_{i,j}$.

Stage 3. Implementation: the best combination is implemented in the STS. The reference values are compared with those obtained from the implemented combination. If the results are not as expected, stage 1 and stage 2 should be reviewed.

V. CASE STUDY

The proposed method is implemented step-by-step in a case study that consists of obtaining the optimal performance for a physical STS. The tracking accuracy should assess the full tracking system performance and should preferably be measured onsite and in real time at the STS location, including the tracking error and the energy consumption.

A. TRACKER CHARACTERIZATION (STAGE 1)

1) SYSTEM IDENTIFICATION

the STS is used as a pointing sensor platform. In particular, a phototransistor sensor was used; this sun sensor model ISS-T60-B0020 with two orthogonal axes, based on MEMS technology, measures the incident angle of a sun ray and has a high sensitivity with a low power consumption. The main features of the sensor include the two-axis detection (azimuthal and elevation axes) with 120° field of view, sensitivity less than 0.06°, and the average current consumption of 33 mA. Due to the wide field of vision of the sensor, a symmetrical acceptance angle is defined as $\alpha_\beta = \alpha_\gamma = \pm 0.25°$, which considers the average range of other pointing sensors and solar applications, such as photovoltaic and concentration systems. Fig. 3 shows the STS used. The STS has a two-axis configuration in the azimuthal-elevation arrangement. For the tracking action, it has an open-loop configuration with the possibility of implementing various ephemeris algorithms. The hardware of the STS is described below. For data processing, ATMega 2560 is used, with 54 digital I/O ports, 16 analog I/O ports, 8 KB of SRAM memory, 4 KB of EEPROM memory, 5 VDC operating voltage, and six sleep modes. The sleep mode activates and deactivates functions of the processing hardware during a period or an established action, and each mode has configurations to obtain various levels of energy consumption. For measurement of the axis angles, two incremental rotatory encoders are used, with 1, 024 pulses per revolution, 5 VDC input voltage, up to 200 kHz response frequency, and 50 mA current consumption. For the movement of the axes, two geared

Algorithm 1 Heuristic Optimization

```
Initialize i = 1, j = 1, n = 0, and m = 0;
Propose p possible ESS and q possible TS;
for i = 1 : p do
    Evaluate ESS_i in EC_{tot,i};
    if ESS_i is feasible then
        Save ESS_i;
        n = n + 1;
        else
            Discard ESS_i
        end
    end
    xxxxxxxxxx
    i = i + 1;
end
for j = 1 : q do
    Evaluate TS_j in ε_{tot,j};
    if TS_j is feasible then
        Save TS_j;
        m = m + 1;
        else
            Discard TS_j
        end
    end
    j = j + 1;
end
Define K_max = n · m;
Initialize K = 1;
Define the weights w_k,  k = 1, 2;
Create a random initial combination C_{ini_{i,j}}
  ∀i = 1, ..., n;  and ∀j = 1, ..., m;
Evaluate C_{ini_{i,j}} in U(C_{ini_{i,j}});
for K = 1 : K_max do
    Create a new random combination C_{new_{i,j}};
    if C_{new_{i,j}} ≠ C_{ini_{i,j}} then
        Evaluate C_{new_{i,j}} in U(C_{new_{i,j}});
        else
            Discard C_{new_{i,j}};
            Create another combination C_{new_{i,j}};
            Evaluate C_{new_{i,j}} in U(C_{new_{i,j}});
        end
    end
    Compare U(C_{ini_{i,j}}) with U(C_{new_{i,j}});
    if U(C_{new_{i,j}}) < U(C_{ini_{i,j}}) then
        Replace C_{ini_{i,j}} with C_{new_{i,j}};
        else
            Discard C_{new_{i,j}}
        end
    end
    K = K + 1;
end
```

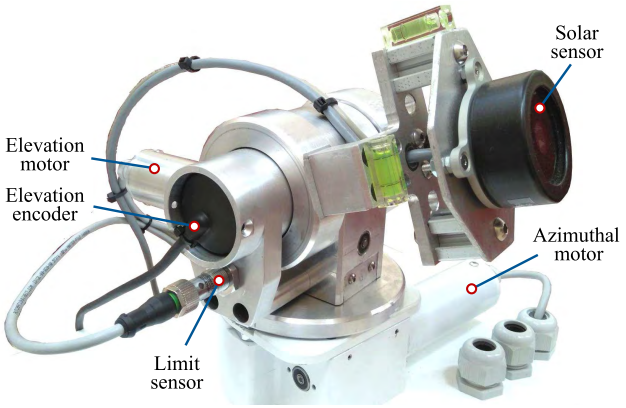

FIGURE 3. Physical two-axis STS for implementation of the proposed optimization approach.

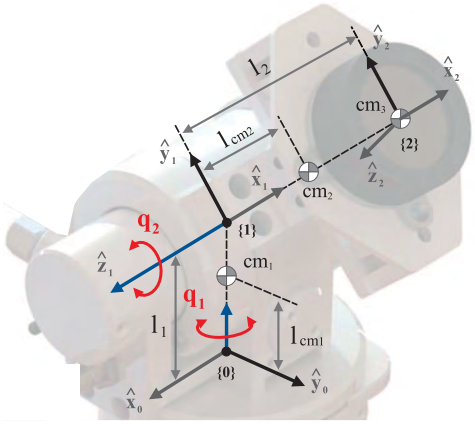

FIGURE 4. Tracking system description. Frame {0} is the base frame, while frame {2} is the solar collector frame and coincides with the center of mass of sun sensor (cm_3).

motors with a gear ratio of 392 and power consumption of 0.54 W are used. In addition, each motor has a worm-gear transmission with the anti-backlash mechanism, and a gear ratio of 70. Based on the DC motor data sheet, the optimal speed is calculated to be 0.2357 deg/s. Finally, other hardware of the STS is as follows: a dual-driver motor for motor control, a DC-to-DC converter for power conditioning, a real-time clock for measuring the time during the solar position calculation, two optical limit sensors for setting the tracker home position, and two relative humidity and temperature sensors for the environmental measures.

2) TRACKER MODELING

The kinematic and the dynamic models of the tracker are developed. Fig. 4 shows the frames used to generate the models. Based on [51], the dynamics of the system can be described by the following equations:

$$D(q)\ddot{q} + C(q,\dot{q})\dot{q} + g(q) = \tau \tag{9}$$

where $q, \dot{q}, \ddot{q} \in \mathbb{R}^2$ are the axis angular position, velocity, and acceleration, respectively. The term $D(q) \in \mathbb{R}^{2\times 2}$ is the effective inertia matrix for the motor, $C(q,\dot{q}) \in \mathbb{R}^{2\times 2}$ is the Coriolis matrix, $g(q) \in \mathbb{R}^2$ stands for the gravitational effect vector, and $\tau \in \mathbb{R}^2$ represents the control input. The explicit values of the model are as follows:

$$D(q) = \begin{bmatrix} m_2 l_{cm_2}^2 C_2^2 + I_{y_1} + I_{x_2} S_2^2 + I_{y_2} C_2^2 & 0 \\ 0 & m_2 l_{cm_2}^2 + I_{z_2} \end{bmatrix}$$

$$C(q,\dot{q}) = \begin{bmatrix} C_{11} & C_{12} \\ C_{21} & C_{22} \end{bmatrix}, \quad g(q) = \begin{bmatrix} 0 \\ m_2 g l_{cm_2} C_2 \end{bmatrix}, \quad \tau = \begin{bmatrix} \tau_1 \\ \tau_2 \end{bmatrix}$$

where $I_i = \text{diag}\{I_{x_i}, I_{y_i}, I_{z_i}\}$, $i = 1, 2$ denotes the tensor of inertia of link i, l_{cm2} is the distance from frame {1} to the center of mass of link 2, m_2 denotes the mass of link 2, $C_{11} = (I_{x_2} - I_{y_2} - m_2 l_{cm_2}^2) C_2 S_2 \dot{q}_2$, $C_{12} = (I_{x_2} - I_{y_2} - m_2 l_{cm_2}^2) C_2 S_2 \dot{q}_1$, $C_{21} = (-I_{x_2} + I_{y_2} + m_2 l_{cm_2}^2) C_2 S_2 \dot{q}_1$, and $C_{22} = 0$ (S_2, C_2 stand for $\sin(q_2)$ and $\cos(q_2)$, respectively). To validate the kinematic and dynamic models, a multibody simulation was carried out.

3) TRACKING REFERENCE VALUES

The ENEA algorithm was implemented based on the hardware capabilities, the required acceptance angle, and the accuracy of the pointing sensor. In [41], the expression used to obtain the solar vector $\bar{S}_S$, and the values of azimuthal and elevation angles are shown. To determine the reference values, the tracking operation was performed during a sunny day. The test was carried out at the Instituto de Energía Solar (IES), in Madrid (Spain), at the latitude of 40.4893° and longitude of −3.6827°. On test date of March 30, 2018, the sunrise was at 08:01:54, the sunset occurred at 20:37:34, and the noon time was at 14:19:23. These times represent a total of 12.5944 hours of sunlight. For the tracking error measurement, the same pointing sensor was used. During the tracking operation, the data collected from the sun sensor was recorded on a laptop using the SolarMems® software. For the energy consumption measurements, a Fluke model 289 true RMS multimeter was used, with the automatic data logger recording three samples per second during the operational period. Samples of voltage and current were obtained, operational and idle times were measured, and the conversion to power and energy was performed later applying the expression (6). The measurement point was the general STS power supply. Thus, the real reference values (R_1) were as follows: the average azimuthal tracking error ε_β was 0.32°, the average elevation tracking error ε_γ was 0.37°, the total tracking error ε_{tot} was 0.4891°, and the real total energy consumption $EC_{tot}(t)$ was 7.5284 Wh.

B. HEURISTIC OPTIMIZATION (STAGE 2)

Algorithm 1 starts with the proposal of the *ESS* and *TS*. In the case of the *ESS*, considering the six energy-saving modes the hardware has, and two activation modes of the tracking system axis (sequential or parallel), twelve possible strategies can be obtained ($p = 12$). For *TS*, considering the features of the hardware and that the actuators are DC motors, three strategies are proposed ($q = 3$): the computer torque control (CTC), the generalized proportional integral (GPI) controller,

TABLE 2. Energy saving strategies.

ESS	Movement	Sleep mode
ESS_1	Sequential	Disabled
ESS_2	Parallel	Disabled
ESS_3	Sequential	Enabled
ESS_4	Parallel	Enabled

and the proportional-integral-derivative (PID) controller. Two of them have already been implemented in STSs, the PID in [52], and the GPI in [51]. To determine if the proposed strategies are feasible, it is mandatory to confirm that they satisfy several constraints. In the case of *ESS*, the following features are verified: active clocks, oscillators, wake-up sources, and the current consumption when the sleep mode is active. Hence, the idle sleep mode was selected, with an energy consumption of 15 mA. Considering the sequential and parallel activation, four feasible *ESS* were identified ($n = 4$), as shown in Table 2. Here, the sequential movement refers to the activation of the azimuthal axis; once the azimuthal position has been reached, the elevation axis moves. Additionally, the parallel activation occurs when the axes move to the desired position at the same time. In comparison, the following features are verified for the *TS*: hardware data processing velocity, quantity of registers and interruptions, number of operations and monitoring parameters, and error ranges. In particular, the last feature was revised so that the error range fulfilled the constraints presented in Section II-B ($\varepsilon_\beta \leq \pm 0.25°$, and $\varepsilon_\gamma \leq \pm 0.25°$). The three proposed strategies comply with the constraints, and each strategy is described below.

TS_1: The CTC is a closed-loop controller that has the features of being globally stable, as well as performing precise linearization using feedback when the system is nonlinear [53], [54]. The model and the implementation of CTC in a two-axis solar tracker presented in [55] were considered. In view of the tracking system dynamic model (Eq. 9) and the desired trajectory q^*, the CTC is expressed in a general form as follows:

$$\tau = D(q)[\ddot{q}^* - K_D(\dot{q} - \dot{q^*}) - K_P(q - q^*)] + C(q, \dot{q})\dot{q} + g(q) \quad (10)$$

where $K_D = \text{diag}\{k_{d1}, k_{d2}\}$, $K_P = \text{diag}\{k_{p1}, k_{p2}\}$, and k_{p1}, k_{p2}, k_{d1} and k_{d2} are real positive tuning parameters that ensure exponential stability of the tracking errors.

For the following schemes, the model (9) is simplified in the sense of independent joint robotic control, i.e., assuming that the gear ratio is sufficiently large to neglect some nonlinearities of the original model. The alternative approximate linear dynamics of the tracker is given as follows:

$$J\ddot{q} + B\dot{q} = u + d \quad (11)$$

where $J \in \mathbb{R}^{2\times 2}$, $J = \text{diag}\{J_1, J_2\}$, $J_1, J_2 > 0$ is the effective inertia matrix, $B \in \mathbb{R}^{2\times 2}$, $B = \text{diag}\{b_1, b_2\}$ represents the linear damping effects, $u \in \mathbb{R}^2$ stands for the input vector, and $d \in \mathbb{R}^2$ denotes the neglected dynamics and nonmodeled terms, which are assumed to be locally constant [56]. Note that for solar tracking systems, it is recommended to assume d to be a local ramp to account for the behavior of wind loads [51], [57]; this assumption is used for the generalized proportional integral control.

TS_2: The GPI controller is a scheme that avoids using the angular velocity measurement (necessary in proportional derivative (PD) and computer torque-based schemes) by means of an algebraic time derivative estimator, known as the integral reconstructor [58]. The resulting scheme can be related to a classic compensation network, and the tuning scheme is of the same nature as PID-like controllers. Further information concerning this scheme can be obtained from [51] and [59], where its implementation is reported. The GPI controller is described by the following expression:

$$\begin{aligned} u_i &= u_i^*(t) - J_i\left(k_{4i}\left(\hat{\dot{q}}_i - \dot{q}_i^*\right) + k_{3i}e_{qi}(t)\right. \\ &\quad + k_{2i}\int_0^t e_{qi}(\tau)d\tau + k_{1i}\int_0^t\int_0^{\tau_1} e_{qi}(\tau_2)d\tau_2 d\tau_1 \\ &\quad \left. + k_{0i}\int_0^t\int_0^{\tau_1}\int_0^{\tau_2} e_{qi}(\tau_3)d\tau_3 d\tau_2 d\tau_1\right) \\ e_{qi}(t) &:= q_i(t) - q_i^*(t) \\ \hat{\dot{q}}_i &= \frac{1}{J_i}\left(-B_i q_i + \int_0^t u_i(\tau)d\tau\right) \\ u_i^* &= J_i\ddot{q}_i^* + b_i\dot{q}_i^* \end{aligned} \quad (12)$$

where u_i is the i-th term of u, and $k_{3i}, k_{2i}, k_{1i}, k_{0i} \in \mathbb{R}$ are the control gains, which are chosen such that the error dynamics characteristic polynomial $P_e(s) = s^5 + ((b_i/J_i) + k_{4i})s^4 + k_{3i}s^3 + k_{2i}s^2 + k_{1i}s + k_{0i}$ is a Hurwitz polynomial.

TS_3: Using the simplified model (11), the structure of the application of the PID control allows obtaining acceptable results. The proportional term generates a corrective control action proportional to the tracking error; the integral term generates a control action proportional to the integral of the tracking error, and the derivative term generates a control action proportional to the change in the tracking error range. In [60] and [61], the implementation of the PID is shown for two-axis solar trackers, with tracking errors inside the required limits. The general model of the PID is expressed as follows:

$$u(t) = K_p e(t) + \frac{K_i}{T_i}\int_0^t e(\tau)d\tau + K_d T_d \dot{e}(t) \quad (13)$$

Therefore, the maximum number of combinations is $K_{max} = 12$. Due to the application of the STS, the tracking error and the energy consumption have the same importance; therefore, the weights are defined as $w_1 = w_2 = 0.5$. However, the following process of the Algorithm 1 pertaining to generation and evaluation of the combinations $C_{i,j}$ is carried out using a numerical simulation described below.

Numerical Simulation: the combinations $C_{i,j}$ are the composition of ESS_i with TS_j, where $i = 1, \ldots, 4$ and

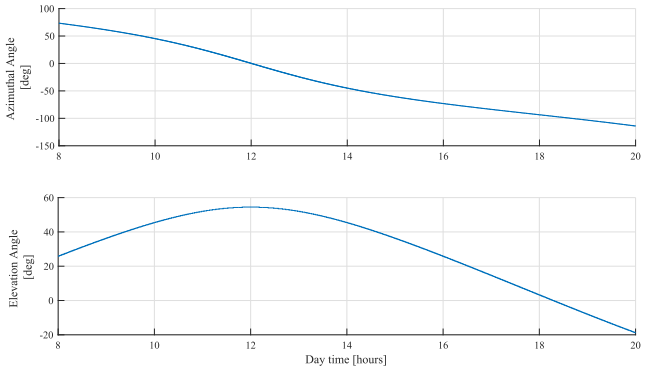

FIGURE 5. Simulation of the solar path segmentation for $\varepsilon_\beta = \varepsilon_\gamma = 0.25°$, and $n_\beta = n_\gamma = 788$.

TABLE 3. Simulation and experimental gains for the TS.

		Simulation		Experimental	
TS	Gain	$u_1(t)$	$u_2(t)$	$u_1(t)$	$u_2(t)$
TS_1	K_D	8,000	30,000	–	–
	K_P	1,000	4,000	–	–
TS_2	k_0	5,000	5,000	4,485	4,358
	k_1	3,100	3,100	2,622	2,715
	k_2	2,500	2,500	2,292	2,062
	k_3	1,000	1,000	1,026	872
	k_4	150	150	122	137
TS_3	K_p	1,500	1,500	–	–
	K_i	10	10	–	–
	K_d	200	200	–	–

TABLE 4. Summary of the tracking errors in simulation.

TS	ε_β			ε_γ			ε_{tot}
	Min	Max	Avg	Min	Max	Avg	
TS_1	−0.05	0.11	0.08	1.6	1.82	1.71	1.1719
TS_2	−0.06	0.06	0.06	−0.05	0.07	0.06	0.0849
TS_3	−0.8	0.8	0.8	0.20	0.40	0.3	0.8544

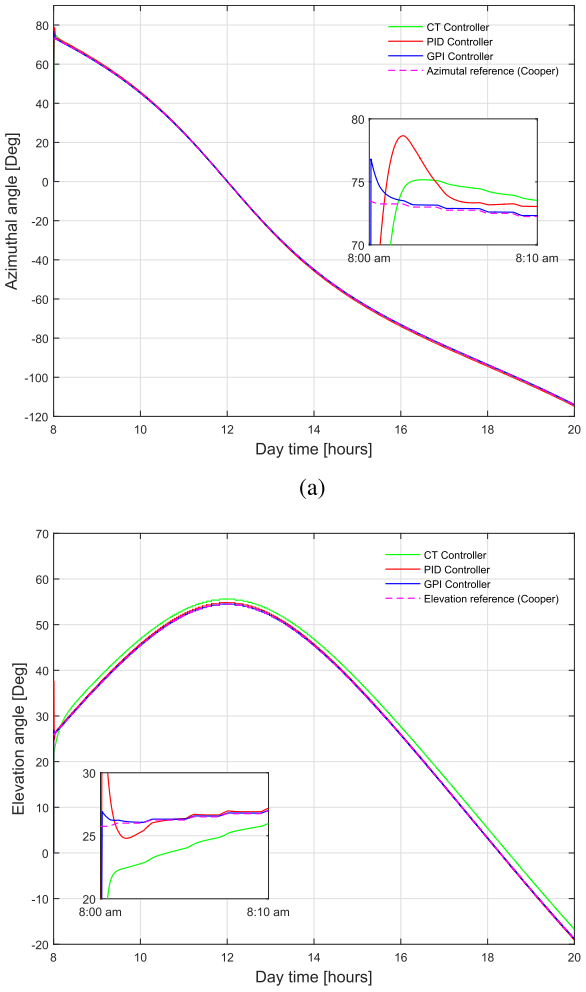

FIGURE 6. Simulation of *TS* strategies, (a) trajectory tracking of the azimuthal movement, and (b) trajectory tracking of the elevation movement. Both including a magnified view of trajectories.

$j = 1, \ldots, 3$. For the simulation analysis, Madrid, Spain, on April 3, 2018, is considered. On that date, the sunrise was at 06:54:05, the sunset occurred at 19:42:28, and the noon time was at 13:18:16, representing a total of 12.8063 hours of sunlight. Considering that the acceptance angles are $\alpha_\beta = \alpha_\gamma = 0.25°$, the total displacement of azimuthal angle is $\beta_{tot} = 196.94°$, and the total elevation angle is $\gamma_{tot} = 108.34°$. Expression (1) is applied to segment the solar path into 788 and into 434 steps for the azimuthal and the elevation movements, respectively. For simplicity in the implementation stage, the number of points in the trajectory are defined as $n_\beta = n_\gamma = 788$. Fig. 5 shows the segmentation of the trajectory in n-points of the azimuthal angle β and the elevation angle γ. Fig. 6a and Fig. 6b show the azimuthal and elevation simulations of the tracking trajectory along the path, implementing the three *TS* strategies, respectively. Fig. 7 shows the tracking error of the azimuthal and elevation angles for each *TS*. The results presented in Fig. 7 are summarized in Table 4. Table 3 shows the values of the gains for the simulations of the TS. Expression (4) is applied to determine the total tracking error ε_{tot}. The TS_2 strategy has the lower tracking error, with a value of 0.0849°. For the time in which it converges to the desired position, the error peaks are considered for each step and are interpreted as additional joint movement to reach the position. Considering that TS_2 has the smallest peak magnitude, it is considered as 100% of the movement time. Then, TS_1 represents 270%, and TS_3 represents 210% of the movement time. Considering the calculated optimal speed, each path step takes 1.06 s. The mean average step-by-step movement time is 2.862 s for TS_1, 1.06 s for TS_2, and 2.226 s for TS_3. The calculation of the energy consumption was performed independently for each axis and hardware device; in the case study, equation (6) can be expressed for each change of the azimuthal and elevation angles. Then, the total energy consumption in the sun tracking system $EC_{tot}(t)$, for n-trajectory points, is calculated by (14):

$$EC_{tot}(t) = EC_1(\tau) + EC_2(\tau) + EC_3(t_{op}) \qquad (14)$$

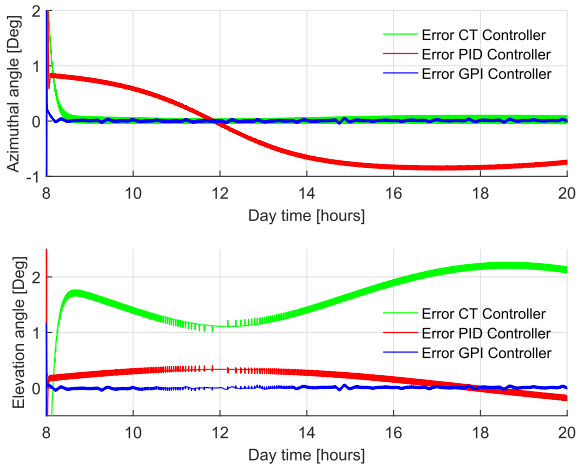

FIGURE 7. Tracking error for the tracking trajectory.

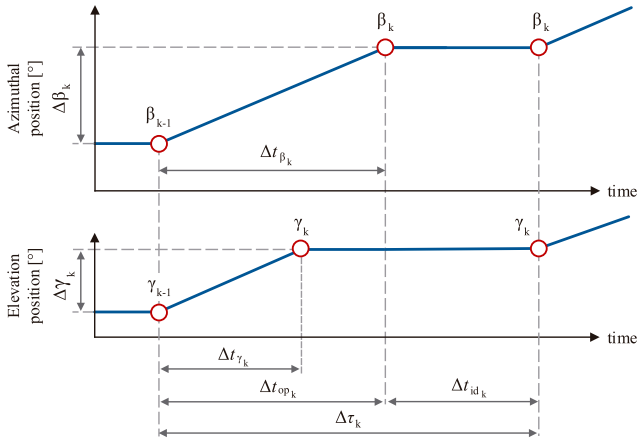

FIGURE 8. Intervals of time for the tracking movement from point.

where $EC_1(\tau)$ is the EC of the data processing hardware. $EC_2(\tau)$ is the EC of the STS hardware devices, described in Section V-A. And, $EC_3(t_{op})$ is the EC for both axis motors. The time intervals for the tracking movement from position $\bar{S}_{k-1}$ to $\bar{S}_k$ are shown in Fig. 8. The total time of daily cycle of tracking τ is the sum of the k-th intervals of operation times Δt_{op_k} and idle times Δt_{id_k}. Considering the n-points of the path and the corresponding time intervals (see Fig.8), the EC of expression (14) are defined below. $EC_1(\tau)$ can be calculated by (15):

$$EC_1(\tau) = EC_{11}(t_{op}) + EC_{12}(t_{id}) \tag{15}$$

Thus, the EC of the processing hardware can be defined in terms of their electrical power $P_p(\tau)$, and calculated by (16) and (17):

$$EC_{11}(t_{op}) = \sum_{k=1}^{n} \int_{\Delta t_{op_k}} |P_p(\tau)| d\tau \tag{16}$$

$$EC_{12}(t_{id}) = \sum_{k=1}^{n} \int_{\Delta t_{id_k}} |P_p(\tau)| d\tau \tag{17}$$

Also, the $EC_2(\tau)$, can be defined by (18)

$$EC_2(\tau) = \sum_{k=1}^{n} \int_{\Delta \tau_k} |P_{hd}(\tau)| d\tau \tag{18}$$

The $EC_3(t_{op})$, can be expressed as a sum of the azimuthal energy consumption $EC_\beta(t_{op})$ and the elevation energy consumption $EC_\gamma(t_{op})$ (19):

$$EC_3(t_{op}) = EC_\beta(t_{op}) + EC_\gamma(t_{op}) \tag{19}$$

Hence, the $EC_\beta(t_{op})$ can be defined by (20):

$$EC_\beta(t_{op}) = \sum_{k=1}^{n_\beta} EC_\beta(\Delta t_{\beta_k}) + EC_{\beta_0}(\Delta t_{\beta_0})$$

$$EC_\beta(t_{op}) = \sum_{k=1}^{n_\beta} \int_{\Delta t_{\beta_k}} |P_\beta(\tau)| d\tau + \int_{t_{\beta_n}}^{t_{\beta_0}} |P_\beta(\tau)| d\tau \tag{20}$$

where $EC_{\beta_0}(\Delta t_{\beta_0})$ is the EC in the STS required to return the system into its azimuthal initial position; Δt_{β_0} is the time interval of the movement from the position β_n to the initial position β_0; and $P_\beta(\tau)$ is the electrical power of the azimuthal axis. As well as, the EC_γ can be calculated by (21):

$$EC_\gamma(t_{op}) = \sum_{k=1}^{n_\gamma} EC_\gamma(\Delta t_{\gamma_k}) + EC_{\gamma_0}(\Delta t_{\gamma_0})$$

$$EC_\gamma(t_{op}) = \sum_{k=1}^{n_\gamma} \int_{\Delta t_{\gamma_k}} |P_\gamma(\tau)| d\tau + \int_{t_{\gamma_n}}^{t_{\gamma_0}} |P_\gamma(\tau)| d\tau \tag{21}$$

where $EC_{\gamma_0}(\Delta t_{\gamma_0})$ is the EC required to return the system into its elevation initial position; Δt_{γ_0} is the time interval of the movement from the position γ_n to the initial position γ_0; and $P_\gamma(\tau)$ is the electrical power of the elevation axis. $\bar{S}_{k-1}(\beta_{k-1}, \gamma_{k-1})$ to $\bar{S}_k(\beta_k, \gamma_k)$. The energy saving efficiency for each combination was calculated using the expression (8). Fig.9 shows a bar graph with the results of the EC simulation and calculation for all combinations. Note that the energy consumed by the system during the idle periods has a significant impact on the total energy consumption. The tracking errors were obtained from the numerical simulations, the mixed error was obtained using the expression (3), and equation (4) is applied to determine the total tracking error. The simulation results are summarized in Table 5, including the simulation of the reference combination ($\hat{R}_1$). The energy unit is Watt-hour (Wh), and the error unit is degree (°). The best combination $C_{4,2}$, composed of the GPI controller and ESS_4, has the minimum value of the utility function at 4.6232. The energy saving efficiency is 0.3155; the total energy consumption is 9.16160834 Wh; and the total tracking error is 0.0848°.

C. IMPLEMENTATION (STAGE 3)

The better three combinations ($C_{2,2}$, $C_{3,2}$, and $C_{4,2}$) from the simulation test were implemented in the STS and also tested in the IES. The test date for $C_{2,2}$ combination was April 1, 2018; April 2, 2018 for $C_{3,2}$; and April 3, 2018,

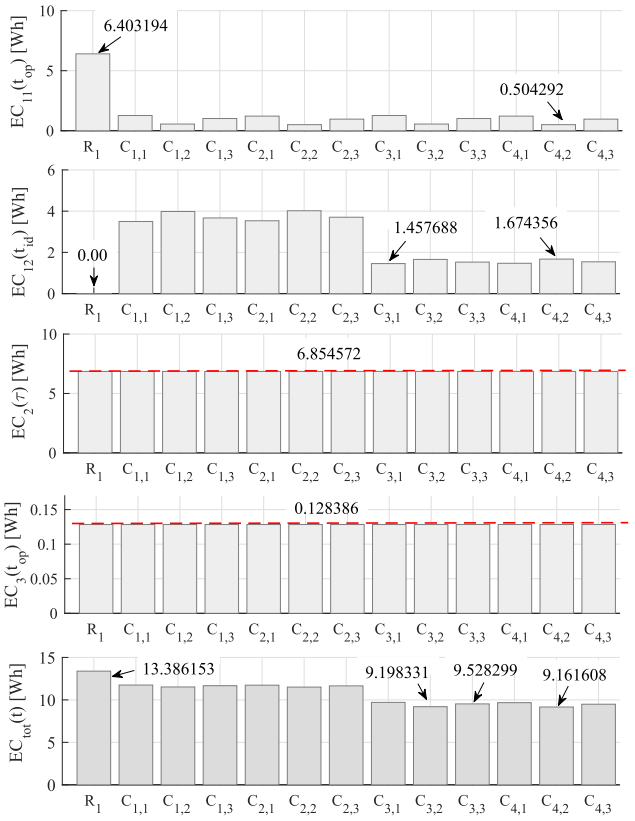

FIGURE 9. Bar graph from the EC simulation results of the reference R_1 and the $C_{i,j}$ combinations.

for the combination $C_{4,2}$. All tracking data were the same data matched that of the numerical simulation. For the measurement of the parameters, a system called experimental measurement system (EMS) was developed. The EMS was used to measure the electrical current and voltage at four points of the STS while keeping record of the real positions of each movement axis and the solar pointing sensor positions. The electrical power measures were the general power supply ($P_s(\tau)$), the power of the azimuthal axis ($P_\beta(\tau)$), the power of the elevation axis ($P_\gamma(\gamma)$), and the power of the processing hardware device ($P_p(\tau)$). Fig. 10 shows the connection scheme between the STS and the EMS. β_e and γ_e are the measures of the azimuthal and elevation encoders, respectively. The associated power measurement variables of the scheme are the following: MS_1 deals with the power supply, MS_2 is oriented to the processing hardware device, MS_3 for the consumption of the azimuthal axis, and MS_4 for elevation axis respectively. The EMS is composed of current and voltage sensors, the SolarMems sensor, and a measurement drive responsible for the total energy consumption calculation and the constant recording of time. The chosen current and voltage sensors are of model ACS712, which has a total output error of 1.5%, single 5.0 VDC supply operation and 5 A direct current support. The measurement drive is an ATMega-2560 microcontroller. The analog-to-digital converter yields the resolution between readings of 0.0049 V

TABLE 5. Summarized simulation and calculation results of $C_{i,j}$ combinations, from Fig. 9.

	Units	$\hat{R}_1$	$C_{1,1}$	$C_{1,2}$	$C_{1,3}$	$C_{2,1}$	$C_{2,2}$	$C_{2,3}$	$C_{3,1}$	$C_{3,2}$	$C_{3,3}$	$C_{4,1}$	$C_{4,2}$	$C_{4,3}$
$EC_{11}(t_{op})$	Wh	6.4031	1.2676	0.5555	1.0163	1.2163	0.5042	0.9650	1.2676	0.5555	1.0163	1.2163	0.5042	0.9650
$EC_{12}(t_{id})$	Wh	0	3.4991	3.9842	3.6703	3.5340	4.0192	3.7053	1.4576	1.6598	1.5290	1.4722	1.6743	1.5435
$EC_2(\tau)$	Wh	6.8545	6.8545	6.8545	6.8545	6.8545	6.8545	6.8545	6.8545	6.8545	6.8545	6.8545	6.8545	6.8545
$EC_3(t_{op})$	Wh	0.1283	0.1283	0.1283	0.1283	0.1283	0.1283	0.1283	0.1283	0.1283	0.1283	0.1283	0.1283	0.1283
$EC_{tot}(t)$	Wh	13.3861	11.7497	11.5228	11.6696	11.7333	11.5064	11.6533	9.7082	9.1983	9.5282	9.6715	9.1616	94915
$\eta(C_{i,j})$	-	0	0.1222	0.1391	0.1282	0.1234	0.1404	0.1294	0.2747	0.3128	0.2881	0.2774	0.3155	0.2909
ε_β	°	0.32	0.08	0.06	0.8	0.08	0.06	0.8	0.08	0.06	0.8	0.08	0.06	0.8
ε_γ	°	0.37	1.71	0.06	0.3	1.71	0.06	0.3	1.71	0.06	0.3	1.71	0.06	0.3
ε_{tot}	°	0.4891	1.7118	0.0848	0.8544	1.7118	0.0848	0.8544	1.7118	0.0848	0.8544	1.7118	0.0848	0.8544
$U(C_{i,j})$	-	6.9376	6.7307	5.8038	6.2620	6.7226	5.7956	6.2538	5.7100	4.6415	5.1913	5.6917	4.6232	5.1729

(4.9 mV) per unit, or 5 V/1, 024 units. The maximum sampling time is 1×10^{-4} s or 0.0001 seconds. For the recording of data in real time, a 16 GB microSD memory card connected to the measurement drive was used by the microSD module. For each test, the total energy consumption $EC_{tot}(t)$ in the STS is calculated by (14), (16), (17), (18), (20), and (21)

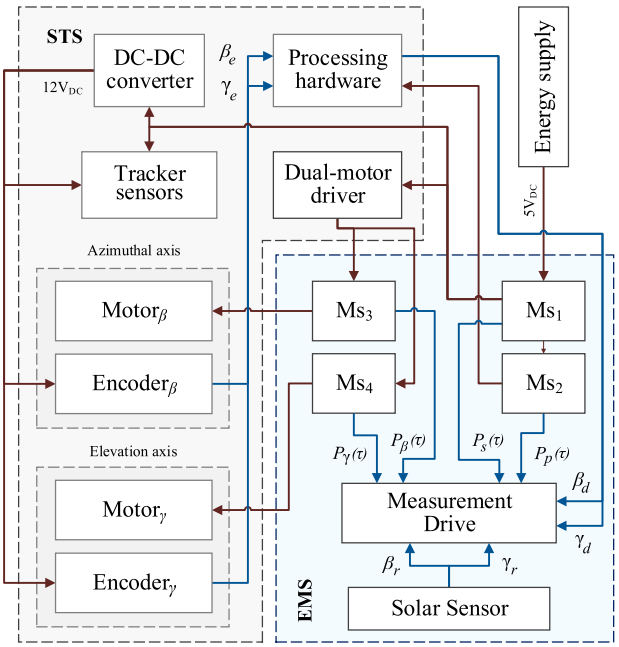

FIGURE 10. Connection scheme between STS and EMS.

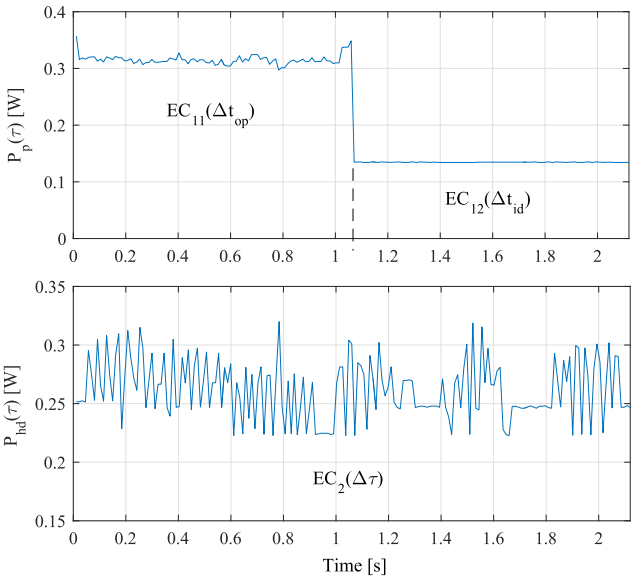

FIGURE 11. Experimental EC of the data processing hardware $EC_1(\tau)$, and EC of the hardware devices $EC_2(\tau)$ for the movement of one step trajectory.

using the measured voltages and currents, and the recorded time intervals. Expression (22) is applied to the determine the electrical power of the hardware devices $P_{hd}(\tau)$, given by:

$$P_{hd}(\tau) = P_s(\tau) - P_p(\tau) - P_\beta(\tau) - P_\gamma(\tau) \qquad (22)$$

Fig. 13 shows a bar graph with the experimental results of the EC and calculation for the tested combinations. The best energy saving combination is the same as the obtained in simulation results, the combination $C_{4,2}$. The real total EC was 5.4966 Wh. The experimental results of $P_p(\tau)$ and

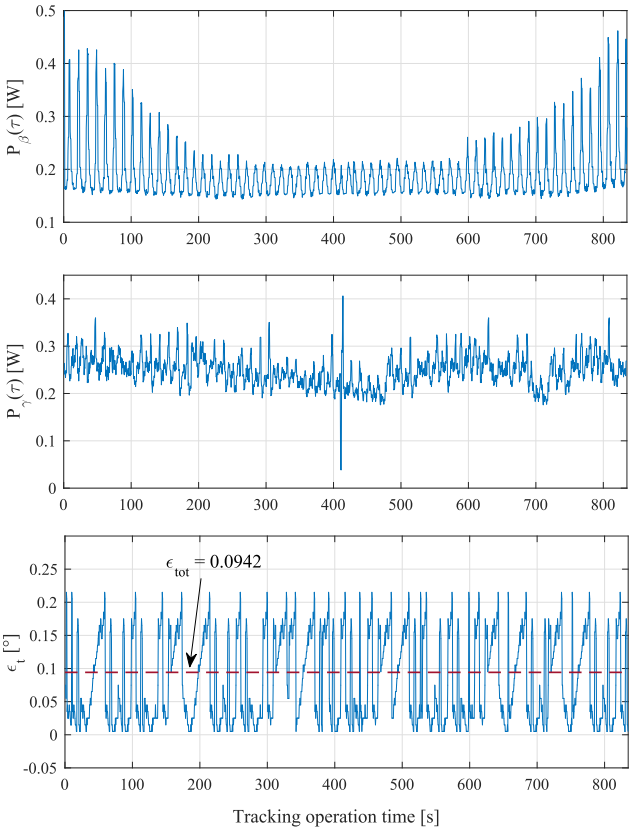

FIGURE 12. Experimental EC of the azimuthal axis $EC_\beta(t_{op})$ and elevation axis $EC_\gamma(t_{op})$, and mixed tracking error ε_t.

TABLE 6. Summarized experimental results of $C_{2,2}$, $C_{3,2}$, $C_{4,2}$ and R_1 combinations, from Fig. 13.

	Units	R_1	$C_{2,2}$	$C_{3,2}$	$C_{4,2}$
$EC_{11}(t_{op})$	Wh	4.0229	0.3168	0.3490	0.3168
$EC_{12}(t_{id})$	Wh	0	4.0192	1.6598	1.6743
$EC_2(\tau)$	Wh	3.4563	3.4563	3.4563	3.4563
$EC_3(t_{op})$	Wh	0.0491	0.0491	0.0491	0.0491
$EC_{tot}(t)$	Wh	7.5284	7.8415	5.5143	5.4966
$\eta(C_{i,j})$	-	0	-0.0415	0.2675	0.2698
ε_β	°	0.32	0.059	0.062	0.062
ε_γ	°	0.37	0.065	0.069	0.071
ε_{tot}	°	0.48	0.0878	0.0928	0.0942
$U(C_{i,j})$	-	4.0088	3.9632	2.7996	2.7907

$P_{hd}(\tau)$ for the movement of one step trajectory are given in Fig. 11. The activation of the energy saving mode is clearly appreciated once the desired point has been reached at time around 1.06s. Fig. 12 shows the experimental results of the EC of the azimuthal and elevation axes of the complete trajectory. The measurement of the tracking error is performed by the pointing sensor to obtain the real angles, the azimuthal real angle (β_r), and the elevation real angle (γ_r). The desired

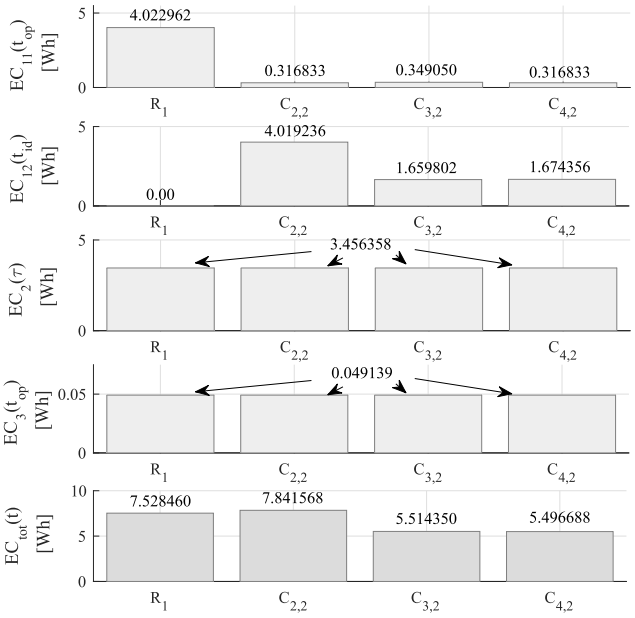

FIGURE 13. Bar graph from the EC experimental results of the reference R_1, $C_{2,2}$, $C_{3,2}$, and $C_{4,2}$ combinations.

tracking angles (β_d and γ_d) are obtained from the solar trajectory calculated with the ENEA algorithm. Expressions (2), (3), and (4) are used to calculate the total tracking error. For $C_{4,2}$ combination, the average azimuthal tracking error was 0.062°; the average elevation tracking error was 0.071°; and the total tracking error was 0.0942. Fig. 12 shows the mixed tracking error along the whole trajectory, and the total tracking error. The experimental results are summarized in Table 6. Table 3 shows the values of the TS-gains for the experimental tests. Finally, considering the reference values presented earlier, and applying the expression (8), the real energy saving efficiency was 0.2698.

VI. CONCLUSIONS AND FUTURE WORK

In this research, a novel methodology for a strategy with low energy consumption and high accuracy in solar applications was proposed, following a heuristic approach. This approach provided an alternative solution to the existing compromise between the tracking accuracy and the energy consumption in STSs by stating and solving an optimization problem. The values obtained from the simulations are close to the real values, allowing the implementation of this approach in larger systems without affecting their productivity, due the trustworthiness of the methodology. In the case study, 26.98% of energy is saved during the tracking action, which represents saving 2.0318 Wh. If an STS with the lifetime of 10 years is considered, with an average of 7.94 hours of sunlight per day in Madrid, the proposed approach will save 58.92 kW. Finally, the utility function allows obtaining the best combination of strategies for STS, finding a harmonic balance between the tracking error and the energy savings and adjusting the balance according to the application that the STS will perform.

ACKNOWLEDGMENTS

The authors express special gratitude to the Universidad Politécnica de Madrid and the Instituto de Energía Solar for the support provided for the experimental tests. The author D. A. Flores-Hernández would like to thank the laboratory technician Eduardo Hernández-Lira for providing CNC machining advice and manufacturing several solar tracker parts.

REFERENCES

[1] *Annual Energy Outlook 2007, With Projections to 2030*, U.S. Dept. Energy, Washington, DC, USA: Energy Inf. Admin., 2007.
[2] *Annual Energy Outlook 2018, With Projections to 2050*, U.S. Dept. Energy, Washington, DC, USA: Energy Inf. Admin., 2018.
[3] G. H. Bauer, *Photovoltaic Solar Energy Conversion*, vol. 901. Berlin, Germany: Springer, 2015.
[4] M. Shabani and J. Mahmoudimehr, "Techno-economic role of PV tracking technology in a hybrid PV-hydroelectric standalone power system," *Appl. Energy*, vol. 212, pp. 84–108, Feb. 2018.
[5] T. P. Chang, "Output energy of a photovoltaic module mounted on a single-axis tracking system," *Appl. Energy*, vol. 86, no. 10, pp. 2071–2078, 2009.
[6] E. Yin, Q. Li, and Y. Xuan, "Optimal design method for concentrating photovoltaic-thermoelectric hybrid system," *Appl. Energy*, vol. 226, pp. 320–329, Sep. 2018.
[7] C. Alexandru, "A novel open-loop tracking strategy for photovoltaic systems," *Sci. World J.*, vol. 2013, Sep. 2013, Art. no. 205396.
[8] J. P. Castillo, C. D. Mafiolis, E. C. Escobar, A. G. Barrientos, and R. V. Segura, "Design, construction and implementation of a low cost solar-wind hybrid energy system," *IEEE Latin Amer. Trans.*, vol. 13, no. 10, pp. 3304–3309, Oct. 2015.
[9] S. Seme and G. Štumberger, "A novel prediction algorithm for solar angles using solar radiation and differential evolution for dual-axis sun tracking purposes," *Sol. Energy*, vol. 85, no. 11, pp. 2757–2770, 2011.
[10] S. Seme, G. Štumberger, and J. Voršič, "Maximum efficiency trajectories of a two-axis sun tracking system determined considering tracking system consumption," *IEEE Trans. Power Electron.*, vol. 26, no. 4, pp. 1280–1290, Apr. 2011.
[11] K.-Y. Lee *et al.*, "A novel algorithm for single-axis maximum power generation sun trackers," *Energy Convers. Manage.*, vol. 149, pp. 543–552, Oct. 2017.
[12] A. Battezzato, S. Mauro, and C. Scarzella, "Developing a parallel kinematic solar tracker for HCPV," in *Proc. ASME 11th Biennial Conf. Eng. Syst. Design Anal.*, 2012, pp. 459–464.
[13] F. Cruz-Peragón, P. J. Casanova-Peláez, F. A. Díaz, R. López-García, and J. M. Palomar, "An approach to evaluate the energy advantage of two axes solar tracking systems in Spain," *Appl. Energy*, vol. 88, no. 12, pp. 5131–5142, 2011.
[14] C. Alexandru, "Optimizing the control system of a single-axis sun tracking mechanism," in *Proc. MATEC Web Conf.*, vol. 184, 2018, pp. 1–4.
[15] H. Fathabadi, "Novel high accurate sensorless dual-axis solar tracking system controlled by maximum power point tracking unit of photovoltaic systems," *Appl. Energy*, vol. 173, pp. 448–459, Jul. 2016.
[16] S. Ahmad, S. Shafie, and M. Z. A. Ab Kadir, "Power feasibility of a low power consumption solar tracker," *Procedia Environ. Sci.*, vol. 17, pp. 494–502, Jan. 2013.
[17] G. C. Lazaroiu, M. Longo, M. Roscia, and M. Pagano, "Comparative analysis of fixed and sun tracking low power PV systems considering energy consumption," *Energy Convers. Manage.*, vol. 92, pp. 143–148, Mar. 2015.
[18] C. Domínguez, N. Jost, S. Askins, M. Victoria, and I. Antón, "A review of the promises and challenges of micro-concentrator photovoltaics," in *Proc. AIP Conf.*, vol. 1881, no. 1, 2017, pp. 1–6.
[19] G. Prinsloo and R. Dobson, *Solar Tracking: Sun Position, Sun Tracking, Sun Following*. Stellenbosch, South Africa: Prinsloo, 2015.
[20] M. M. Abu-Khader, O. O. Badran, and S. Abdallah, "Evaluating multi-axes sun-tracking system at different modes of operation in Jordan," *Renew. Sustain. Energy Rev.*, vol. 12, no. 3, pp. 864–873, 2008.
[21] M. Sarker, M. R. Pervez, and R. Beg, "Design, fabrication and experimental study of a novel two-axis sun tracker," *Int. J. Mech. Mechatron. Eng.*, vol. 10, no. 1, pp. 13–18, 2010.

[22] B. Gupta, N. Sonkar, B. S. Bhalavi, and P. J. Edla, "Design, construction and effectiveness analysis of hybrid automatic solar tracking system for amorphous and crystalline solar cells," *Amer. J. Eng. Res.*, vol. 2, no. 10, pp. 221–228, 2013.

[23] M. Ghassoul, "Design of an automatic solar tracking system to maximize energy extraction," *Int. J. Emerg. Technol. Adv. Eng.*, vol. 3, no. 5, pp. 453–460, 2013.

[24] M. S. Sabry, "Determining the accuracy of solar trackers," M.S. dissertation, Dept. Tech. Environ. Des., Appalachian State Univ., Boone, NC, USA, Aug. 2013.

[25] T. Noguchi, S. Togashi, and R. Nakamoto, "Short-current pulse-based maximum-power-point tracking method for multiple photovoltaic-and-converter module system," *IEEE Trans. Ind. Electron.*, vol. 49, no. 1, pp. 217–223, Feb. 2002.

[26] E. Koutroulis, K. Kalaitzakis, and N. C. Voulgaris, "Development of a microcontroller-based, photovoltaic maximum power point tracking control system," *IEEE Trans. Power Electron.*, vol. 16, no. 1, pp. 46–54, Jan. 2001.

[27] I.-S. Kim, "Robust maximum power point tracker using sliding mode controller for the three-phase grid-connected photovoltaic system," *Sol. Energy*, vol. 81, no. 3, pp. 405–414, 2007.

[28] J. Ahmed and Z. Salam, "An improved perturb and observe (P&O) maximum power point tracking (MPPT) algorithm for higher efficiency," *Appl. Energy*, vol. 150, pp. 97–108, Jul. 2015.

[29] Y.-Y. Hong, A. A. Beltran, and A. C. Paglinawan, "A robust design of maximum power point tracking using Taguchi method for stand-alone PV system," *Appl. Energy*, vol. 211, pp. 50–63, Feb. 2018.

[30] C.-Y. Lee, P.-C. Chou, C.-M. Chiang, and C.-F. Lin, "Sun tracking systems: A review," *Sensors*, vol. 9, no. 5, pp. 3875–3890, 2009.

[31] P. I. Cooper, "The absorption of radiation in solar stills," *Sol. Energy*, vol. 12, no. 3, pp. 333–346, 1969.

[32] J. W. Spencer, "Fourier series representation of the position of the sun," *Search*, vol. 2, no. 5, p. 172, 1971.

[33] L. W. Swift, Jr., "Algorithm for solar radiation on mountain slopes," *Water Resour. Res.*, vol. 12, no. 1, pp. 108–112, 1976.

[34] C. L. Pitman and L. L. Vant-Hull, "Errors in locating the sun and their effect on solar intensity predictions," in *Proc. Meeting Amer. Sect. Int. Sol. Energy Soc.*, Denver, CO, USA, vol. 28, 1978, pp. 701–706.

[35] R. Walraven, "Calculating the position of the sun," *Sol. Energy*, vol. 20, no. 5, pp. 393–397, 1978.

[36] C. B. Archer, "Comments on 'calculating the position of the sun,'" *Sol. Energy*, vol. 25, no. 1, p. 91, 1980.

[37] P. G. Holland and I. Mayer, "On calculating the position of the sun," *Int. J. Ambient Energy*, vol. 9, no. 1, pp. 47–52, 1988.

[38] J. J. Michalsky, "The Astronomical Almanac's algorithm for approximate solar position (1950–2050)," *Sol. Energy*, vol. 40, no. 3, pp. 227–235, 1988.

[39] M. Blanco-Muriel, D. C. Alarcón-Padilla, T. López-Moratalla, and M. Lara-Coira, "Computing the solar vector," *Sol. Energy*, vol. 70, no. 5, pp. 431–441, 2001.

[40] I. Reda and A. Andreas, "Solar position algorithm for solar radiation applications," *Sol. Energy*, vol. 76, no. 5, pp. 577–589, Jan. 2004.

[41] R. Grena, "An algorithm for the computation of the solar position," *Sol. Energy*, vol. 82, no. 5, pp. 462–470, 2008.

[42] R. Grena, "Five new algorithms for the computation of sun position from 2010 to 2110," *Sol. Energy*, vol. 86, no. 5, pp. 1323–1337, 2012.

[43] M. V. Pérez, "New concepts and techniques for the development of high-efficiency concentrating photovoltaic modules," Ph.D. dissertation, Dept. de Electrónica Física, Universidad Politécnica de Madrid, Madrid, Spain, May 2014.

[44] B. Stafford, M. Davis, J. Chambers, M. Martínez, and D. Sanchez, "Tracker accuracy: Field experience, analysis, and correlation with meteorological conditions," in *Proc. 34th IEEE Photovoltaic Spec. Conf. (PVSC)*, Jun. 2009, pp. 2256–2259.

[45] E. Mezura-Montes, M. Reyes-Sierra, and C. A. C. Coello, "Multi-objective optimization using differential evolution: A survey of the state-of-the-art," in *Advances in Differential Evolution*. Berlin, Germany: Springer, 2008, pp. 173–196.

[46] S. S. Rao, *Engineering Optimization: Theory and Practice*. New York, NJ, USA: Wiley, 2009.

[47] M. G. Villarreal-Cervantes, A. Rodríguez-Molina, C.-V. García-Mendoza, O. Peñaloza-Mejía, and G. Sepúlveda-Cervantes, "Multi-objective on-line optimization approach for the DC motor controller tuning using differential evolution," *IEEE Access*, vol. 5, pp. 20393–20407, 2017.

[48] R. T. Marler and J. S. Arora, "The weighted sum method for multi-objective optimization: New insights," *Struct. Multidisciplinary Optim.*, vol. 41, no. 6, pp. 853–862, 2010.

[49] T. L. Saaty, "Decision making with the analytic hierarchy process," *Int. J. Services Sci.*, vol. 1, no. 1, pp. 83–98, 2008.

[50] I. Kaliszewski and D. Podkopaev, "Simple additive weighting—A metamodel for multiple criteria decision analysis methods," *Expert Syst. Appl.*, vol. 54, pp. 155–161, Jul. 2016.

[51] D. Flores-Hernández, S. Palomino-Resendiz, N. Lozada-Castillo, A. Luviano-Juárez, and I. Chairez, "Mechatronic design and implementation of a two axes sun tracking photovoltaic system driven by a robotic sensor," *Mechatronics*, vol. 47, pp. 148–159, Nov. 2017.

[52] R. Garrido and A. Díaz, "Cascade closed-loop control of solar trackers applied to HCPV systems," *Renew. Energy*, vol. 97, pp. 689–696, Nov. 2016.

[53] M. W. Spong and M. Vidyasagar, *Robot Dynamics and Control*. Hoboken, NJ, USA: Wiley, 2008.

[54] H. Sira-Ramírez, R. Márquez, F. Rivas-Echevarría, and O. Llanes-Santiago, *Control de Sistemas no Lineales: Linealización Aproximada*. Upper Saddle River, NJ, USA: Prentice-Hall, 2005.

[55] S. I. Palomino-Resendiz, D. A. Flores-Hernández, A. Luviano-Juárez, N. Lozada-Castillo, and I. Chairez-Oria, "Control por par calculado para un seguidor solar de dos grados de libertad," in *Mecatrónica y Robótica de Servicio: Teoría y Aplicaciones*. Santiago de Querétaro, Mexico: Asociación Mexicana de Mecatrónica A.C., 2016, ch. 10, pp. 98–110.

[56] M. W. Spong, S. Hutchinson, and M. Vidyasagar, *Robot Modeling and Control*. New York, NY, USA: Wiley, 2006.

[57] J. Tomczyk, J. Cink, and A. Kosucki, "Dynamics of an overhead crane under a wind disturbance condition," *Automat. Construct.*, vol. 42, pp. 100–111, Jun. 2014.

[58] M. Fliess, R. Marquez, E. Delaleau, and H. Sira-Ramírez, "Correcteurs proportionnels-intégraux généralisés," *ESAIM, Control, Optim. Calculus Variat.*, vol. 7, pp. 23–41, Jan. 2002.

[59] S. Palomino-Resendiz, D. Flores-Hernández, N. Lozada-Castillo, L. Guzmán-Vargas, and A. Luviano-Juárez, "Design and implementation of a robotic active solar distiller based on a Fresnel concentrator and a photovoltaic system," *Energy Convers. Manage.*, vol. 166, pp. 637–647, Jun. 2018.

[60] A. Yazidi, F. Betin, G. Notton, and G. A. Capolino, "Low cost two-axis solar tracker with high precision positioning," in *Proc. 1st Int. Symp. Environ. Identities Medit. Area*, Jul. 2006, pp. 211–216.

[61] S. Ozcelik, H. Prakash, and R. Challoo, "Two-axis solar tracker analysis and control for maximum power generation," *Procedia Comput. Sci.*, vol. 6, pp. 457–462, Jan. 2011.

DIEGO A. FLORES-HERNÁNDEZ was born in Mexico City, in 1987. He received the B.S. degree in mechatronic engineering from Unidad Profesional Interdisciplinaria en Ingeniería y Tecnologías Avanzadas (UPIITA-IPN), Mexico City, in 2005, the M.S. degree in manufacturing engineering from ESIME-IPN, Mexico City, in 2009, the MBA degree from the Universidad Tecnológica de México, in 2016, and the Ph.D. degree in robotic and mechatronic systems engineering from CIDETEC-IPN, Mexico City, in 2018. Since 2010, he has been a full-time Professor with the Advanced Technology Department, UPIITA-IPN. His research interests include design and manufacturing mechatronic and robotic systems, optimization theory, and design methodologies.

SERGIO I. PALOMINO-RESENDIZ received the degree in communications and electronics engineering from the National Polytechnic Institute (IPN), Mexico City, Mexico, in 2014, and the master's degree in advanced technology from the Interdisciplinary Professional Unit on Engineering and Advanced Technologies, IPN, in 2017, where he is currently pursuing the Ph.D. degree in advanced technologies. His research interests are the design and control of mechatronic systems oriented to Photovoltaic energy collection and storing as well as the use of solar energy as thermal generators.

ALBERTO LUVIANO-JUÁREZ received the B.S. degree in mechatronics engineering from the National Polytechnic Institute (IPN), Mexico City, Mexico, in 2003, the M.Sc. degree in automatic control from the Department of Automatic Control, Center of Investigation and Advanced Researching (CINVESTAV), IPN, in 2006, and the Ph.D. degree in electrical engineering from the Department of Electrical Engineering, CINVESTAV, in 2011. He is currently with the Postgraduate and Research Section, Interdisciplinary Professional Unit on Engineering and Advanced Technologies, IPN. His current research interests include robust estimation and control in mechatronic systems, and algebraic methods in the estimation and control of nonlinear systems.

NORMA LOZADA-CASTILLO received the degree from the Superior School of Physics and Mathematics (ESFM), National Polytechnic Institute (IPN), and the master's and Ph.D. degrees from the Automatic Control Department, CINVESTAV, IPN. Her research interests include stochastic control, and non-linear control and estimation in stochastic systems.

OCTAVIO GUTIÉRREZ-FRÍAS was born in Mexico City. He received the B.S. degree in mechatronics from the Professional School of Engineering and Advanced Technologies, National Polytechnic Institute of Mexico (UPIITA-IPN), in 2003, the M.S. degree in computing engineering from the Computing Research Center, National Polytechnic Institute, in 2006, and the Ph.D. degree in computer sciences from CIC-IPN, in 2009. Since 2011, his researches focus on control of nonlinear systems, underactuated systems, robotics, and automation.